A technique optimization protocol and the potential for dose reduction in digital mammography

Nicole T. Ranger[a)]
Department of Radiology, Carl E. Ravin Advanced Imaging Laboratories, Duke University, Durham, North Carolina 27710

Joseph Y. Lo
Department of Radiology and Department of Biomedical Engineering, Carl E. Ravin Advanced Imaging Laboratories, Duke University, Durham, North Carolina 27710

Ehsan Samei
Department of Radiology, Department of Biomedical Engineering, and Department of Physics, Carl E. Ravin Advanced Imaging Laboratories, Duke University, Durham, North Carolina 27710

(Received 16 January 2009; revised 12 November 2009; accepted for publication 27 November 2009; published 4 February 2010)

Digital mammography requires revisiting techniques that have been optimized for prior screen/film mammography systems. The objective of the study was to determine optimized radiographic technique for a digital mammography system and demonstrate the potential for dose reduction in comparison to the clinically established techniques based on screen- film. An objective figure of merit (FOM) was employed to evaluate a direct-conversion amorphous selenium (*a*-Se) FFDM system (Siemens Mammomat *Novation*^{DR}, Siemens AG Medical Solutions, Erlangen, Germany) and was derived from the quotient of the squared signal-difference-to-noise ratio to mean glandular dose, for various combinations of technique factors and breast phantom configurations including kilovoltage settings (23–35 kVp), target/filter combinations (Mo–Mo and W–Rh), breast-equivalent plastic in various thicknesses (2–8 cm) and densities (100% adipose, 50% adipose/50% glandular, and 100% glandular), and simulated mass and calcification lesions. When using a W–Rh spectrum, the optimized FOM results for the simulated mass and calcification lesions showed highly consistent trends with kVp for each combination of breast density and thickness. The optimized kVp ranged from 26 kVp for 2 cm 100% adipose breasts to 30 kVp for 8 cm 100% glandular breasts. The use of the optimized W–Rh technique compared to standard Mo–Mo techniques provided dose savings ranging from 9% for 2 cm thick, 100% adipose breasts, to 63% for 6 cm thick, 100% glandular breasts, and for breasts with a 50% adipose/50% glandular composition, from 12% for 2 cm thick breasts up to 57% for 8 cm thick breasts. © *2010 American Association of Physicists in Medicine*. [DOI: 10.1118/1.3276732]

Key words: digital mammography, image quality, figure of merit, technique optimization, dose reduction

I. INTRODUCTION

In recent years, there have been significant advancements in breast imaging including positron emission mammography, contrast-enhanced breast MRI, dedicated breast CT, and breast tomosynthesis. Nevertheless, conventional screening x-ray mammography is arguably still the most cost effective and practical diagnostic imaging tool for the early diagnosis of breast cancer. Until relatively recently, the only options for performing screening mammography studies were analog screen/film breast imaging systems, which, despite their high spatial resolution, suffer from limitations in latitude and display contrast, detection efficiency, storage, dissemination, and operating efficiency.[1–3] With the advent of new digital mammography imaging systems, most of these limitations have been overcome due to the high detection efficiency and wide dynamic range of new detectors and the practical efficiencies achieved with digital imaging.[1] Digital mammography also provides exciting opportunities for advanced mammographic imaging applications including, but not limited to, advanced image processing and CAD, tomosynthesis, contrast-enhanced dual energy subtraction mammography, multimodality image fusion, and stereo visualization techniques.[4–7] Furthermore, unlike mammography based on analog screen/film for which the functions of detection, storage, and display are all achieved using the analog film, in digital mammography systems, these functions are performed separately, enabling the independent optimization of the system's acquisition, storage, and display stages. Specifically, the introduction of digital mammography systems has necessitated revisiting the issue of screening mammography technique optimization, given the removal of constraints imposed by the narrow latitude of screen/film systems and associated requirements to match the x-ray spectrum and exposure to the response characteristics of mammographic film.

For a digital mammography system with a high detection efficiency, the spectral quality of the x-ray beam has a strong

effect on diagnostic quality because as has been previously established,[1,8] detectability of low-contrast breast masses will be most limited by low-contrast resolution or low signal-to-noise ratio. As the intrinsic image contrast to noise ratio (CNR), also known as the signal-difference-to-noise ratio (SdNR), is strongly correlated with exposure and dose, an objective image quality metric should incorporate the CNR (or SdNR) normalized by the mean glandular dose (MGD). The $SdNR^2$ can be measured using breast-equivalent phantoms in various configurations, while glandular dose can be estimated using spectral simulation models that incorporate the known incident exposure, spectral characteristics (target, filter, kVp, and HVL), and relevant breast phantom characteristics (thickness and glandular fraction).

The current study aimed to evaluate the potential dose savings achievable in the migration from prior techniques based on a Mo–Mo spectrum optimized for analog screen-film to new optimized techniques for digital mammography based on a W–Rh spectrum using an objective figure of merit (FOM) equal to the $SdNR^2$ normalized by MGD. This FOM was evaluated for both Mo–Mo and W–Rh target/filter combinations for breast thicknesses of 2–8 cm with various glandular compositions using a clinical *a*-Se full-field digital mammography (FFDM) system. The data were used to assess the dependency of system performance on spectral quality and draw conclusions regarding the achievable dose savings in the migration to new optimized techniques specific to digital mammography.

II. METHODS

II.A. Imaging system

The imaging device employed for this evaluation was an investigational amorphous selenium (*a*-Se) FFDM system, which has subsequently been commercialized (Siemens Mammomat *Novation*^{DR}, Siemens AG Medical Solutions, Erlangen, Germany). The system employs Mo–Mo, Mo–Rh, and W–Rh target/filter combinations with a 30 μm Mo filter, a 25 μm Rh filter, and a 50 μm Rh filter, respectively. For purely logistical reasons and because the W/Rh target filter combination is recommended by the manufacturer, our evaluation employed both the W–Rh target/filter combination in addition to the Mo–Mo target/filter combination since Mo–Mo has historically been associated with screen/film mammography; Mo–Rh was not employed during this study in order to reduce the burden of data collection. The detector was comprised of a 23.3×28.7 cm^2 direct-conversion *a*-Se flat panel array employing a 250 μm thick *a*-Se layer with a pixel pitch of 70 μm and an output image dimension of 3328 pixels $\times$ 4096 pixels. The characteristics of this investigational system have been previously described.[9] Prior to the study, the system was calibrated per the manufacturer's recommended protocol using a Mo–Mo technique with a tube kilovoltage of 28 kVp at 250 mAs with 4 cm of polymethyl methacrylate (PMMA) placed at the tube exit window. The calibration and all subsequently acquired image data were acquired with the antiscatter grid in place. The grid had a 5:31 grid ratio and was comprised of lead with paper interspacing. All images were corrected for the detector gain and offset variations and defective detector elements but were not subjected to application-specific image processing, i.e., the DICOM tag for presentation state was "for processing."

Comparisons were made to a reference Mo–Mo technique that was derived from a pre-existing clinical technique table for screen-film mammography systems (Siemens *MAMMOMAT 3000 Nova*, Siemens AG Medical Solutions, Erlangen, Germany) in use at this institution. This technique table is based on a screen-film system that has identical generator, target/filter combinations, and gantry geometry as the above FFDM system.

II.B. Breast phantom setup

To simulate breast imaging conditions, slabs of ICRU-44 (Ref. 10) compliant breast-equivalent plastic (CIRS, Inc., Norfolk, VA), with densities simulating 100% adipose, 50% adipose/50% glandular, and 100% glandular tissue, were used to achieve simulated breast thicknesses of 2, 4, 6, and 8 cm. For a given breast thickness, stacks of each of the three breast density slabs were positioned at the detector edge corresponding to the chest wall [Fig. 1(a)] to be imaged

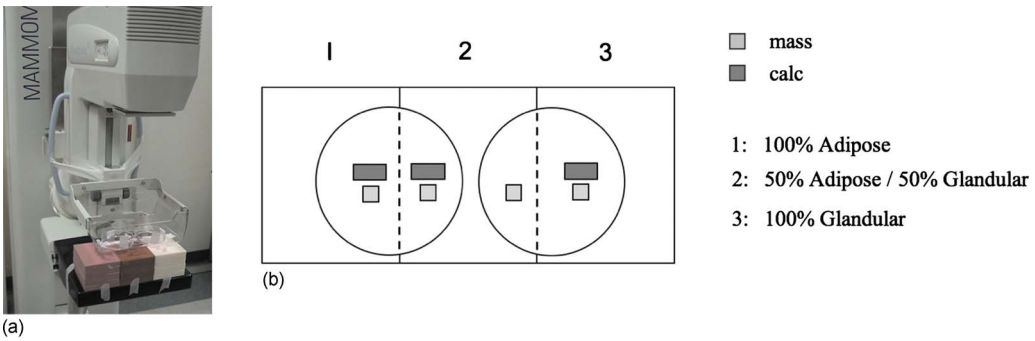

FIG. 1. (a) Photograph showing the FFDM imaging system used in this evaluation (Siemens Mammomat *Novation*^{DR}, Siemens Medical Systems) and the phantom configuration employed for evaluation of the FOM. Three breast compositions (100% adipose, 50% adipose/50% glandular, and 100% glandular) were imaged simultaneously in thicknesses of 2, 4, 6, and 8 cm. A large compression paddle was used to support petri dishes containing oil and simulated mass and calcium inclusions [see Fig. 1(b)]. (b) Overhead schematic of the relative position of mass and calcium simulated lesions with respect to the breast phantom.

TABLE I. Measured HVL at each spectral condition.

Kilovoltage (kVp)	HVL (mm Al)	
	Mo–Mo	W–Rh
23	0.249	0.453
26	0.332	0.483
28	0.354	0.503
30	0.373	0.515
32	0.386	0.531
35	0.407	0.551

simultaneously. Lesion inclusions comprised of muscle-equivalent plastic with a 100% glandular composition measuring $10.5\times10.5\times5$ mm thick (CIRS, Inc., Norfolk, VA) used to simulate breast masses and inclusions of bone-equivalent plastic measuring $30.0\times10.0\times0.35$ mm thick (GAMMEX RMI, Middleton, WI) used to simulate calcifications were placed above a compression paddle at a fixed height of 11 cm from the detector cover, with one mass and one calcification inclusion per stack of breast composite material [Fig. 1(b)]. The lesions were embedded in a small volume of triglyceride vegetable oil, corresponding to approximately 5 mm depth, to simulate the approximate contrast that would be obtained with the same lesion embedded in breast-equivalent material.

II.C. Data acquisition

To estimate breast phantom entrance exposure at each spectral condition, exposure measurements were performed free-in-air with a calibrated ionization detector with a dedicated mammography probe (Radcal 1515/10X5-6M, Radcal Corporation, Monrovia, CA) positioned 8 cm above the detector centered on the chest wall axis with a spacing of 2.4 cm from the chest wall. Measurements using Mo–Mo and W–Rh target/filter combinations at 23, 26, 28, 30, 32, and 35 kVp were acquired at 250 mAs. To correlate these measurements with subsequently acquired image data, exposures were linearly scaled to the applicable mAs condition being evaluated and then geometrically extrapolated to the phantom surface using the inverse square law to reflect the actual surface entrance exposure. Using narrow beam conditions, the half-value layer (HVL) for each of the spectral combinations was separately evaluated using the mammo probe positioned at 4.5 cm from the detector using 2–6, 0.1 mm Al filters placed in a compression paddle at a distance of 18 cm from the detector surface. The HVL results, tabulated in Table I, were used for the estimation of the MGD (noted below).

TABLE II. Technique variables employed for this evaluation.

Study parameter	No. of variable	Description
Target/filter	2	Mo–Mo, W–Rh
kVp settings	6	23, 26, 28, 30, 32, 35
Breast phantom composition	3	100% adipose, 50% adipose/50% glandular, 100% glandular
Breast thickness	4	2, 4, 6, and 8 cm
Inclusions (mass and calcification)	2	With, without

TABLE III. Optimized radiographic technique for FFDM using W–Rh target/filter determined from FOM results of the current study using an investigational *a*-Se FFDM system (Siemens Mammomat *Novation*^{DR}, Siemens Medical System). The results reported are for masses and calcifications (calcification results are shown in parentheses).

Optimized radiographic technique for FFDM using W–Rh spectrum			
	Breast phantom composition		
Breast thickness (cm)	Adipose (kVp)	Mixed (50–50) (kVp)	Glandular (kVp)
2	26 (27)	28 (28)	29 (29)
4	27 (28)	29 (29)	29 (29)
6	29 (29)	29 (29)	29 (29)
8	30 (30)	30 (30)	30 (29)

The breast phantom configuration was imaged in two conditions: With and without inclusions [Figs. 1(a) and 1(b) and Table II]. For each phantom condition, using all spectral combinations (Mo–Mo and W–Rh at 23, 26, 28, 30, 32, and 35 kVp) and for each phantom thickness (2, 4, 6, and 8 cm), images were acquired at an mAs chosen to yield a target mean pixel value of 300–350 where possible (actual range: 150–700) in background regions of interest overlying each of the three simulated breast densities. These target pixel values are based on the mean count obtained in a region of interest (ROI) overlying breast tissue, when the system automatic exposure control (AEC) device is utilized. The corresponding surface entrance exposure was computed as previously described.

II.D. Analysis

The mean glandular dose for each spectral condition was computed using a modified version of the *Spectrum* algorithm[11,12] to accommodate a Rh filter thickness of 50 μm (default=25 μm for W/Rh). The spectrum algorithm computes MGD based on the known target/filter combination, the measured HVL and entrance surface exposure for the spectrum of interest, and the breast phantom thickness and percentage glandular composition.

The squared signal-difference-to-noise ratio ($SdNR^2$) was computed separately for the mass and calcification inclusions from the difference in mean pixel value of a 2.8×2.8 mm^2 (Ref. 13) region of interest located at the same coordinates in the images with and without inclusions divided by the standard deviation of the region without inclusions, obtained at the same exposure level. Though these images were obtained at approximately the same exposure level, a slight correction to account for the small fluctuations in x-ray flux that are typical of sequential xray exposures was made based on the relative counts in an equally sized region of interest beyond the phantom, located in the background area corresponding

to unattenuated beam; that correction was applied to the signal and background deduced from the ROI analysis of the images with inclusions, before computing $SdNR^2$. The figure of merit was then computed from the ratio of the squared signal-difference-to-noise ratio to the mean glandular dose for each spectral combination, breast composition (density) type, and thickness.[2]

Due to inherent fluctuations in the FOM raw data, a two-stage fitting technique was employed to estimate a "computed-from-fit" FOM for the purposes of dose comparisons. First, the optimized kVp technique was established by constructing a technique chart for W–Rh (Table III) based on a second-order surface polynomial fit to the plot of the FOM original data (z axis) versus kVp (x axis) and thickness (y axis). For each breast composition, the kVp associated with the maximized FOM estimate at a given breast thickness was determined from the second-order polynomial surface fitting function. This second-order surface fit captured the trending in FOM as a function of the breast thickness and kVp quite well, yielding consistent values of the kVp associated with the maximized FOM estimate from comparison of fit versus FOM original data, but in some cases significantly over- or underestimated the actual FOM values. For this reason, a separate fit based on the 2D plot of FOM original data value versus kVp was utilized for the purpose of estimating the final FOM computed-from-fit. This was accomplished by applying a third-order polynomial fit to the plot of FOM original data versus kVp and solving for FOM using the optimized kVp technique, previously determined (Table III).

In a similar fashion, for Mo–Mo the FOM computed-from-fit values corresponding to recommended technique (kVps) (Table IV) based on this institution's clinical technique charts for screen-film mammography were determined from a third-order polynomial fit to the plot of FOM original data versus kVp. For a given breast density/thickness, the ratio of the optimized computed-from-fit FOM for W–Rh to

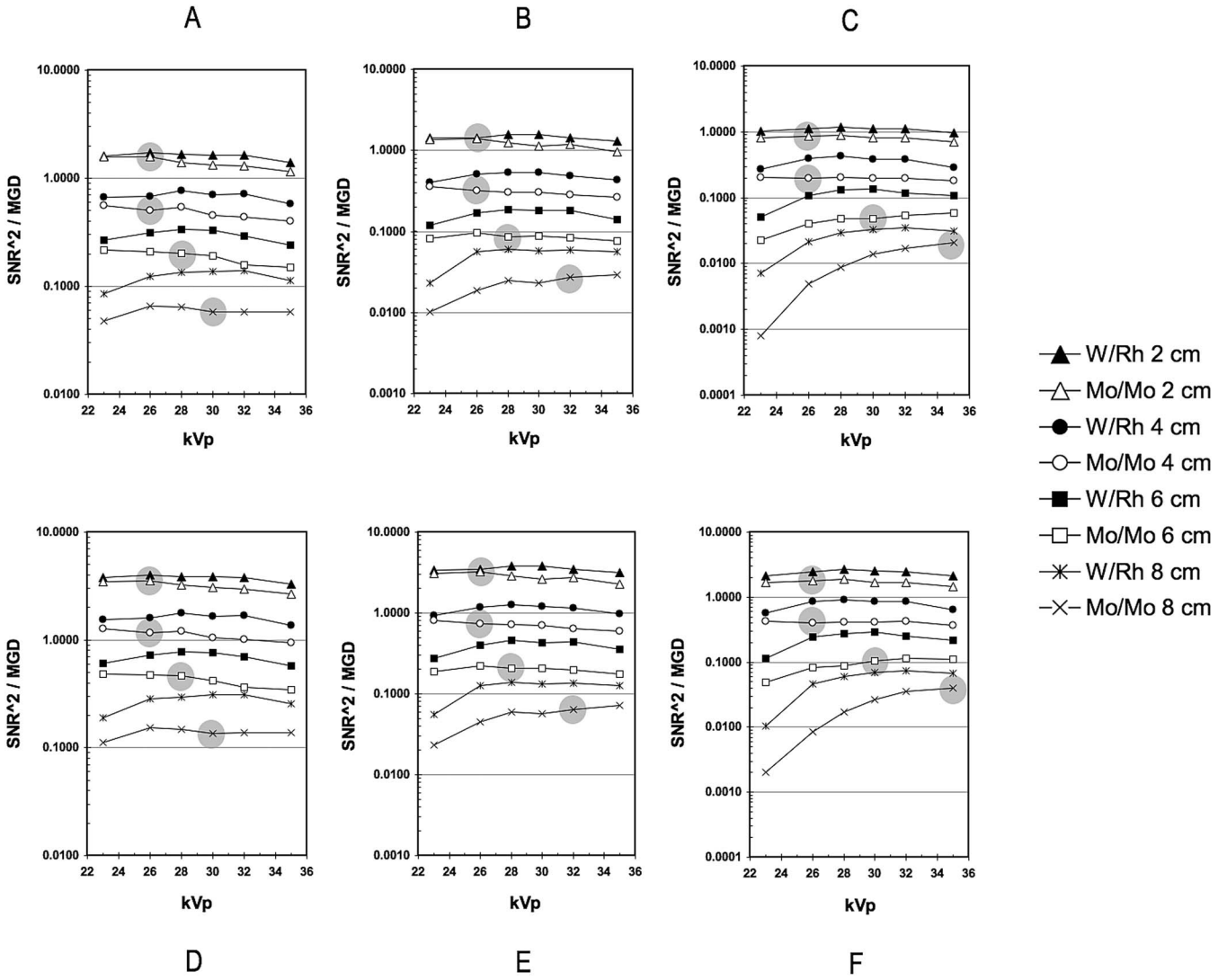

FIG. 2. [(a)–(f)] Graphs showing the relationship between the FOM and kVp for both Mo–Mo and W–Rh target/filter combinations for 100% adipose [(a) and (d)], 50% adipose/50% glandular [(b) and (e)], and 100% glandular [(c) and (f)]. The FOM, defined by the ratio of $SdNR^2/MGD$, was calculated for both mass [(a)–(c)] and calcification [(d)–(f)] lesions, where SdNR is the signal-difference-to-noise ratio and MGD is the mean glandular dose. The solid gray circles represent the previously established clinical technique based on Mo–Mo and screen/film, shown here for comparison purposes.

the that of Mo–Mo represents the relative change in $SdNR^2$ while preserving dose, i.e., the (squared) increase in the image quality that could be achieved at the same dose by changing from the pre-existing clinical technique to the proposed W–Rh technique. Therefore, the reciprocal of the ratio was used to compute an estimate of the relative dose reduction when using an optimized W–Rh spectrum over the existing clinical technique based on Mo–Mo, that is, the expected dose reduction that is achievable while maintaining comparable image quality.

For Mo–Mo, *slight* adjustments of 1 kVp were made to the pre-existing clinical technique settings (based on the screen-film) for several thickness/density combinations to match the *specific* kVps used in this study, i.e., 23, 26, 28, 30, 32, and 35 kVp. In addition, certain thickest and densest breast phantom combinations (e.g., 8 cm thickness, 100% glandular composition), typically imaged with a Mo–Rh technique clinically, were imaged with the closest matching Mo–Mo technique to simplify the protocol.

III. RESULTS

III.A. FOM results

The FOM results obtained for calcification inclusions were factors of 1.5–2.5 and 1.6–2.6 greater than those obtained for mass inclusions, for W–Rh and Mo–Mo, respectively. However, both demonstrated similar trends, that is, the relative variation in FOM with kVp for both calcification and mass lesions at each target/filter combination was highly consistent (Fig. 2). In general, the FOM varied slowly with kVp. However, for both Mo–Mo and W–Rh with an 8 cm, 100% glandular breast phantom thickness, FOM results decreased markedly in the low kVp range.

The measured optimized technique using Mo–Mo on the digital mammography system was in good agreement with an existing clinical technique using film/screen and Mo–Mo (Fig. 2).

As expected, for a given technique and phantom thickness, the W–Rh spectrum yielded peak FOM results that were consistently higher than those obtained using the reference Mo–Mo spectrum by factors of 1.1–2.3, 1.2–2.2, and 1.4–2.6 for 100% adipose, 50% adipose/50% glandular, and 100% glandular breast compositions, respectively. The trends were generally higher with increasing breast phantom thickness with the exception of the 100% glandular composition where the result obtained showed an uptrend across 2, 4, and 6 cm thicknesses but a downtrend for 8 cm.

III.B. Technique factors

The optimized W–Rh technique settings and pre-existing clinical technique using Mo–Mo are listed in Tables III and IV, respectively. There was an uptrend in kVp setting with increasing breast density for a given thickness and with increasing thickness for a given density. The technique table computed from optimized FOM results obtained using the W–Rh target/filter combination showed the same general trends as that for Mo–Mo, but the range of recommended kVps was narrower with generally only a 0–1 kVp increase in voltage with increasing density or increment in thickness. For W–Rh, at the highest breast densities, 29–30 kVp was determined to be the optimized technique for both mass and calcification lesions.

III.C. Dose reduction

The relative dose reduction expected to be achieved using a W–Rh target/filter combination over a pre-existing clinical technique employing Mo–Mo ranged from 9% to 62% and from 12% to 63% at a constant SdNR for masses and calcifications, respectively, depending on the breast thickness and density (Table V). For all breast compositions, there was a consistent increase in dose savings with increasing breast size. For example, for a 50% adipose–50% glandular breast density, the dose savings increased from 12% to 57% and from 16% to 54% at a constant SdNR for masses and calcifications, respectively, as breast thickness increased from 2 to 8 cm. The same trend was seen with increasing breast density for a given breast thickness, i.e., for a 4 cm thick breast, dose savings increased from 26% to 52% and from 29% to 55% at a constant SdNR for masses and calcifications, respectively, as breast density ranged from 100% adipose to 100% glandular. The only exception to these trends was the thickest (8 cm) and most dense combination (100%

TABLE IV. Clinical technique based on a Mo–Mo target/filter combination for S/F system. Slight adjustments (±1 kVp) were made to match kVp to the nearest actual kVp used for this study. For consistency, at higher breast thicknesses, an equivalent Mo–Mo technique was chosen in place of the Mo–Rh technique in use clinically.

Reference S/F mammography technique using a Mo–Mo spectrum			
	Breast phantom composition		
Breast thickness (cm)	Adipose (kVp)	Mixed (50–50) (kVp)	Glandular (kVp)
2	26	26	26
4	26	26	26
6	28	28	30
8	30	32	35

TABLE V. Dose reduction achieved when using optimized W–Rh technique (Table I) in comparison to the reference clinical Mo–Mo technique (Table II). The results reported are for masses and calcifications (calcification results are shown in parentheses).

Percentage dose savings achieved using optimized W–Rh spectrum vs Mo/Mo			
	Breast phantom composition		
Breast thickness (cm)	Adipose	Mixed (50-50)	Glandular
2	9% (12%)	12% (16%)	26% (30%)
4	26% (29%)	39% (41%)	52% (55%)
6	40% (41%)	51% (49%)	62% (63%)
8	57% (55%)	57% (54%)	38% (41%)

glandular), where the dose savings of 38% for masses (41% for calcifications) was less than the adjacent combinations.

IV. DISCUSSION

A number of investigators demonstrated the potential for dose reduction in digital mammography[2,14–23] using optimized target/filter combinations. This dose reduction may be associated with a loss of contrast that can be compensated for with image processing and digital display systems that enable the manipulation of contrast, making dose reduction a reasonable objective of technique optimization.

In digital mammography, various approaches have been taken to investigate optimized mammographic technique (primarily the choice of beam source target/filter and kVp) for different breast thicknesses and compositions. These include Monte Carlo simulations,[16,24–26] experimental studies using objective image quality metrics,[2,8,14,21,25,27,28] task-based observer evaluations using anthropomorphic and other phantoms with relevant simulated features,[16,17,19,29–31] and even retrospective or prospective clinical mammography studies employing large patient populations.[23] Monte Carlo studies have been particularly useful in permitting practical comparative evaluation of the existing and proposed target/filter combinations for imaging breasts of various thicknesses and densities without requiring an unduly burdensome number of experimental studies. However, Monte Carlo simulation approaches have their limitations and require independent experimental validation. Task-based observer studies must be well designed so that the observation task is diagnostically relevant and not excessively affected by interobserver variability.[29] Clinical mammography evaluations present a challenge in terms of logistics and can be difficult to justify if comparable studies could be performed using reasonable physical simulations of the breast. By comparison, experimental studies employing an objective figure of merit are relatively easy to accomplish and have the advantage of isolating the detector performance from other system components, and thus enable an evaluation of the optimized technique for that detector system, independent of extraneous effects from other system components, e.g., display systems.

The objective of radiographic technique optimization is to establish standardized imaging protocols by determining the optimal trade-off between image quality and dose, which is especially important for screening mammography given the lifetime risk to women who undergo annual mammography examinations. Without evidence that the image quality improvements at a higher dose would guarantee a clinically significant increase in the diagnostic performance, the more conservative route of favoring dose reduction while maintaining acceptable image quality should be followed. For this reason, the primary objective of our evaluation was to determine the potential dose savings achievable using an optimized W–Rh target/filter combination in comparison to the pre-existing clinical technique for screen-film using a Mo–Mo target/filter combination. We demonstrated that significant dose savings (9%–63%) could be achieved with the use of optimized W–Rh spectra in comparison to the pre-existing clinical techniques using Mo–Mo.

As expected for both the Mo–Mo and W–Rh spectra, the figure of merit measured for calcification lesions was markedly higher than that obtained for masses due to the high contrast of calcium relative to soft tissue. Nevertheless, the FOM result trends with kVp for both lesion types were highly consistent, implying that there is no need to make compromises in technique settings to maintain maximum contrast visibility for both masses and calcifications.

The use of a W–Rh target/filter combination provided an improvement in the FOM for the detection of masses and microcalcifications at all breast thicknesses for a 50% adipose/50% glandular breast composition over that obtained using Mo–Mo. This finding was consistent with the results of an independent investigation using the same imaging system.[25] In fact, the recommended kVp values were within 1–2 kVp for all breast thicknesses. However, our study results further demonstrated the improvement in FOM using a W–Rh target/filter combination was also true for 100% adipose and 100% glandular breast compositions. These results are also reasonably consistent with the results of a recently reported study for the same imaging system (Siemens Mammomat *Novation*^{DR})[14] in which a dose savings of 9%–50% was demonstrated using W–Rh in comparison to Mo–Mo using breast phantom thicknesses of 2–7 cm of PMMA and the system's AEC to achieve a target CNR. A different evaluation using the same imaging system[8] employed breast thicknesses of 3, 5, and 7 cm and a W–Rh target/filter combination, and yielded an optimum technique that ranged from 27 kVp for 30% glandular/70% adipose breast composition to 29 kVp for 70% glandular/30% adipose breast composition. These results are reasonably consistent with the results of the current evaluation, taking into account the differences in methodology. Another evaluation[21] employing 2–7 cm thicknesses of PMMA and 0.2 mm Al to simulate contrast demonstrated dose savings of 12%–63% when using a W–Rh spectrum compared to Mo–Mo, which agrees well with the results of the current study. The results of Monte Carlo simulations[24] predicted a W–Rh target/filter combination yields improved image quality over Mo–Mo for calcification lesions and breast thicknesses greater than 2 cm (i.e., 4, 6, 8, and 10 cm only). In comparison, our results showed that W–Rh yields an improved FOM (both masses and calcification lesions) for all breast thicknesses (including 2 cm) and compositions. For calcification lesions and breast thicknesses of 4, 6, and 8 cm with a breast composition of 50% adipose/50% glandular, optimized kilovoltage settings for maximum FOM using W–Rh agreed exactly (28, 29, and 30 kVp, respectively) with those results.

While the results of the current study are useful for predicting the magnitude of dose reduction achievable in the migration from prior optimized clinical techniques based on the Mo–Mo spectra and screen/film to new optimized techniques employing a W–Rh spectrum and an *a*-Se full-field digital mammography system, certain limitations must be acknowledged. The current study was conducted using one

system/detector and the optimized technique for this device will not generally be applicable to systems from other manufacturers; consequently, the relative dose savings using other systems may be different. Nevertheless, the general methodology of this study is applicable to evaluations of other imaging systems and target/filter combinations. For the current study, we limited our evaluation to an optimized W–Rh spectrum relative to a clinical technique based on assumed use of a Mo–Mo spectrum with screen/film system but other spectra historically associated with screen/film systems (Mo–Rh and Rh–Rh) were not evaluated. Due to limited availability of target/filter combinations, we evaluated the prior technique relative to W–Rh only but there are new and proposed target/filter combinations for digital mammography systems that may yield additional improvements in dose and those merit further investigation. The phantoms employed for this evaluation had a uniform background with a noise characteristic that is not a representative of the anatomical background encountered in clinical mammography studies. However, employing a phantom with a more anatomically realistic background would likely not substantially impact the relative dose savings. Furthermore, the mass and calcification inclusions utilized in this evaluation were used to capture the large-area signal response in a limited region of interest, and therefore do not fully reflect the $SdNR^2$ frequency dependency for masses and calcifications encountered clinically. The images employed in this study were "for processing" and did not reflect the impact of application-specific image processing since it was our intent to demonstrate a technique for optimization of the acquisition stage in digital mammography. Even though the impact of image processing for detection tasks in digital mammography is worth studying,[32] the variability in vendor-supplied image processing algorithms, radiologist preference, and the specific detection task at hand will all play an important role in the choice of optimized processing algorithm and parameters. Therefore, image processing and viewing conditions should be separately optimized after optimization of the acquisition stage.

In general, manufacturer recommendations regarding optimized imaging technique should be verified at the time of installation and this is especially true for the current generation of digital mammography imaging systems, many of which employ sophisticated automatic controls (e.g., automatic kVp selection). For these systems, independent manual verification of control devices is necessary and the technique optimization method described herein provides one example of how such a verification might be undertaken.

While there has been recent work in the area of specifying *acceptable* and *achievable* dose limits in digital mammography,[33] specifying recommended dose levels is beyond the scope of this evaluation. However, it should be noted that regional regulatory limits, published *acceptable dose* guidelines or locally established dose levels based on site-specific criteria, can be used as a guide when specifying target mAs/exposure once an optimized technique (target/filter and kVp) has been established. It should also be noted that though the scope of this study does not permit a detailed discussion of procedures for verifying digital mammography automatic exposure control systems, a properly calibrated and stable automatic exposure control system is a prerequisite for the establishment of consistent image quality and dose levels in digital mammography.

V. CONCLUSIONS

Adherence to standardized imaging protocols based on technique optimization studies is especially important in digital mammography because of the lifetime risk to women who undergo periodic mammography examinations and the well-documented tendency for "dose creep" in digital radiography, in general. Thus, for mammography technique optimization, when deciding whether to pursue improved image quality or reduced dose, unless it can be established that the differential increase in dose yields a diagnostically significant improvement in image quality, dose optimization/reduction is an important goal. We have presented a practical and objective methodology for the optimization of mammographic technique and demonstrated that for a digital mammography system, the use of an optimized W–Rh spectrum can yield a significant improvement (9%–63%) in dose over conventional prior techniques, based on a Mo–Mo spectrum and screen film, for breast thicknesses ranging from 2 to 8 cm at compositions ranging from 100% adipose to 100% glandular. Our results further suggest that particularly for very dense breasts greater than or equal to 8 cm thick, there is potential for further spectral optimization using novel target/filter combinations.

ACKNOWLEDGMENTS

The authors wish to thank Jonathan Jesneck and Swatee Singh for their help with the data acquisition, and Martin Tornai and Thomas Boehringer for loan of material and equipment. They also thank Thomas Mertelmeier of Siemens AG for many helpful discussions.

[a]Electronic mail: nicole.ranger@duke.edu

[1]S. Muller, "Full-field digital mammography designed as a complete system," Eur. Radiol. **31**, 25–34 (1997).
[2]E. Samei, J. T. Dobbins III, J. Y. Lo, and M. P. Tornai, "A framework for optimising the radiographic technique in digital x-ray imaging," Radiat. Prot. Dosim. **114**, 220–229 (2005).
[3]E. Samei, R. S. Saunders, Jr., J. A. Baker, and D. M. Delong, "Digital mammography: effects of reduced radiation dose on diagnostic performance," Radiology **243**, 396–404 (2007).
[4]E. D. Pisano and M. J. Yaffe, "Digital mammography," Radiology **234**, 355–362 (2005).
[5]U. Fischer, K. P. Hermann, and F. Baum, "Digital mammography: Current state and future aspects," Eur. J. Radiol. **16**, 38–44 (2006).
[6]C. G. Berman, "Recent advances in breast-specific imaging," Cancer Control **14**, 338–349 (2007).
[7]A. Karellas and V. Srinivasan, "Breast cancer imaging: A perspective for the next decade," Med. Phys. **35**, 4878–4897 (2008).
[8]M. B. Williams, P. Raghunathan, M. J. More, A. Seibert, A. Kwan, J. Lo, E. Samei, N. T. Ranger, L. L. Fajardo, A. McGruder, S. M. McGruder, A. D. A. Maidment, M. J. Yaffe, A. Bloomquist, and G. Mawdsley, "Optimization of exposure parameters in full field digital mammography," Med. Phys. **35**, 2414–2423 (2008).
[9]R. S. Saunders, Jr., E. Samei, J. L. Jesneck, and J. Y. Lo, "Physical characterization of a prototype selenium-based full field digital mammography detector," Med. Phys. **32**, 588–599 (2005).
[10]ICRU, "Tissue substitutes in radiation dosimetry and measurement," International Commission on Radiation Units and Measurements, Report

No. 44 (Bethesda, MD, 1989).
[11]J. M. Boone, "Glandular breast dose for monoenergetic and high-energy x-ray beams: Monte Carlo assessment," Radiology **213**, 23–37 (1999).
[12]J. M. Boone, T. R. Fewell, and R. J. Jennings, "Molybdenum, rhodium, and tungsten anode spectral models using interpolating polynomials with application to mammography," Med. Phys. **24**, 1863–1874 (1997).
[13]A. Alsager, K. C. Young, and J. M. Oduko, "Impact of heel effect and ROI size on the determination of contrast-to-noise ratio for digital mammography systems," Proc. SPIE **6913**, 69134I1–69134I11 (2008).
[14]J. M. Oduko, K. C. Young, O. Gundogdu, and A. Alsager, "Effect of using tungsten-anode x-ray tubes on dose and image quality in full-field digital mammography," in Lecture Notes in Computer Science: Digital Mammography: Proceedings of the 9th International Workshop on Digital Mammography (IWDM), edited by E. Krupinski, Springer-Verlag, Lect. Notes Comput. Sci. **5116**, 522–529 (2008).
[15]C. Kimme-Smith, "New digital mammography systems may require different x-ray spectra and therefore, more general normalized glandular dose values," Radiology **213**, 7–10 (1999).
[16]S. Obenauer, K. P. Hermann, C. Schorn, U. Fischer, and E. Grabbe, "Full-field digital mammography: Dose-dependent detectability of breast lesions and microcalcinosis," Rofo Fortschr Geb Rontgenstr Neuen Bildgeb Verfahr **172**, 1052–1056 (2000).
[17]S. Obenauer, K. P. Hermann, and E. Grabbe, "Dose reduction in full-field digital mammography: an anthropomorphic breast phantom study," Br. J. Radiol. **76**, 478–482 (2003).
[18]M. P. Andre and B. A. Spivey, "Optimization of tungsten x-ray spectra for digital mammography: Comparison of model to experiment," Proc. SPIE **3032**, 411–418 (2004).
[19]G. Gennaro, L. Katz, H. Souchay, C. Alberelli, and C. di Maggio, "Are phantoms useful for predicting the potential of dose reduction in full-field digital mammography?," Phys. Med. Biol. **50**, 1851–1870 (2005).
[20]K. C. Young, J. M. Oduko, H. Bosmans, K. Nijs, and L. Martinez, "Optimal beam quality selection in digital mammography," Br. J. Radiol. **79**, 981–990 (2006).
[21]P. Toroi, F. Zanca, K. C. Young, C. Van Ongeval, G. Marchal, and H. Bosmans, "Experimental investigation on the choice of the tungsten/rhodium anode/filter combination for an amorphous selenium-based digital mammography system," Eur. J. Radiol. **17**, 2368–2375 (2007).
[22]P. Baldelli, N. Phelan, and G. Egan, "Effect of anode/filter combination on the dose and image quality of a digital mammography system based on an amorphous selenium detector," in Lecture Notes in Computer Science: Digital Mammography: Proceedings of the 9th International Workshop on Digital Mammography (IWDM), E. Krupinski, Springer-Verlag, Lect. Notes Comput. Sci. **5116**, 716–723 (2008).
[23]D. F. P. Uhlenbrock and T. Mertelmeier, "Comparison of anode/filter combinations in digital mammography with respect to average dose," Rofo Fortschr Geb Rontgenstr Neuen Bildgeb Verfahr **181**(3), 249–254 (2009).
[24]D. R. Dance, A. K. Thilander, M. Sandborg, C. L. Skinner, I. A. Castellano, and G. A. Carlsson, "Influence of anode/filter material and tube potential on contrast, signal-to-noise ratio and average absorbed dose in mammography: A Monte Carlo study," Br. J. Radiol. **73**, 1056–1067 (2000).
[25]P. Bernhardt, T. Mertelmeier, and M. Hoheisel, "X-ray spectrum optimization of full-field digital mammography: Simulation and phantom study," Med. Phys. **33**, 4337–4349 (2006).
[26]H. Delis, G. Spyrou, L. Costaridou, G. Tzanakos, and G. Panayiotakis, "Suitability of new anode materials in mammography: Dose and subject contrast determinations using Monte Carlo simulation," Med. Phys. **33**, 4221–4235 (2006).
[27]M. B. Williams, M. J. More, V. Venkatakrishnan, L. Niklason, M. J. Yaffe, G. Mawdsley, A. Bloomquist, A. D. A. Maidment, D. Chakraborty, C. Kimme-Smith, and L. Fajardo, "Beam optimization for digital mammography," in Digital Mammography: Proceedings of the 5th International Workshop on Digital Mammography (IWDM), edited by M. J. Yaffe, 108–119 (2000).
[28]M. B. Williams, P. Raghunathan, A. Seibert, A. Kwan, J. Lo, E. Samei, L. Fajardo, A. D. A. Maidment, M. J. Yaffe, and A. Bloomquist, "Beam optimization for digital mammography—II," in Lecture Notes in Computer Science: Digital Mammography: Proceedings of the 8th International Workshop on Digital Mammography (IWDM), M. Astley *et al.*, Springer-Verlag, Lect. Notes Comput. Sci. **4046**, 273–280 (2006).
[29]W. Huda, "How good is the ACR accreditation phantom for assessing image quality in digital mammography," Acad. Radiol. **9**, 764–772 (2002).
[30]M. Ruschin, P. Timberg, M. Bath, B. Hemdal, T. Svahn, R. S. Saunders, E. Samei, I. Andersson, S. Mattsson, D. P. Chakrabort, and A. Tingber, "Dose dependence of mass and microcalcification detection in digital mammography: Free response human observer studies," Med. Phys. **34**, 400–407 (2007).
[31]E. A. Berns, R. E. Hendrick, and G. R. Cutter, "Optimization of technique factors for an amorphous silicon diode array full-field digital mammography system and comparison to screen-film mammography with matched average glandular dose," Med. Phys. **30**, 334–340 (2003).
[32]F. Zanca, J. Jacobs, C. Van Ongeval, F. Claus, V. Celis, C. Geniets, V. Provost, H. Pauwels, G. Marchal, and H. Bosmans, "Evaluation of clinical image processing algorithms used in digital mammography," Med. Phys. **36**, 765–775 (2009).
[33]R. Van Engen, S. Van Woudenberg, H. Bosmans, K. C. Young, and M. Thijssen, "The European protocol for the quality control of the physical and technical aspects of mammography screening. Part B: Digital mammography," *European Guidelines for Breast Cancer Screening*, 4th ed. (European Commission, Luxembourg, 2006).